Highly Accurate and Noise-Robust Phase Delay Estimation using Multitaper Reassignment

Maria Åkesson*, Oskar Keding†, Isabella Reinhold‡ and Maria Sandsten§
Mathematical Statistics, Centre for Mathematical Sciences
Lund University, Lund, Sweden
* Email: maria.akesson@matstat.lu.se
† Email: oskar.keding@matstat.lu.se
‡ Email: isabella.reinhold@matstat.lu.se
§ Email: maria.sandsten@matstat.lu.se

***Abstract*—The recently developed Phase-Scaled Reassignment (PSR) can estimate phase-difference between two oscillating transient signals with high accuracy. However, in low signal-to-noise ratios (SNRs) the performance of commonly applied reassignment techniques is known to deteriorate. In order to reduce variance in low SNR, we propose a multitaper PSR (mtPSR) method for phase-difference estimation between Gaussian transient signals. Three possible variations of this method are investigated and evaluated, mtPSR1, mtPSR2, and mtPSR3. All three variations are shown to outperform state-of-the-art methods and improve estimation accuracy in low SNR. The mtPSR1 is superior in terms of computational efficiency while the mtPSR3 achieves the highest accuracy. The mtPSR technique is also shown to be robust to model assumptions. An example of phase delay estimates of the electrical signals measured from the brain reveals promising results.**

I. Introduction

Time-frequency (TF) methods are essential tools when analysing signals that are multi-component and non-stationary. Many such signals have oscillating structures that carry important information, these signals can be found in various applications, e.g. vibration analysis, radar detection, geophysics, and medicine. For multi-component signals of transient and short amplitude modulated (AM) oscillating structures, we have invented a matched reassigned spectrogram (MRS) technique that sharpens the TF representation of such signals and is used to accurately estimate signal parameters [1]–[4]. For signals with longer frequency modulated (FM) structures, TF sharpening techniques include the TF reassignment [5], [6], and synchrosqueezing [7], which have been further developed in e.g. [8]–[12]. Other reassignment related methods, including filtering techniques, for impulse signals and transient chirps also exist [13], [14].

The phase delay between signals is of interest in many fields, including direction of arrival estimation, source separation and spatio-temporal decoding in neurology and soundscape analysis. The reassigned spectrogram contains no phase information, similar to all quadratic TF representations [15]. However, phase information is contained in the reassignment vectors (RVs) and we have previously expanded the use of RVs into phase estimation techniques for the cross-spectrogram [16]–[19]. These methods are TF local measures of phase synchronisation and can measure the phase delay of transient signal structures more accurately than the commonly used time-based Pearson's linear correlation (CORR), TF cross-spectrogram phase (XSP) [15], and Phase Lag Index [20]. There are phase estimation methods utilising the synchrosqueezing transform, however these methods are designed for longer FM signals [21], [22].

In spectral analysis, multitapers are used to reduce variance of spectra [23] and the Hermite functions are the optimal choice with respect to TF resolution and orthogonality in the TF domain [24]. For the reassignment methods, degradation of the TF location estimates can happen for low SNRs, because the RVs are sensitive to noise. To rectify this we have recently presented a two-window phase reassignment, where multitapers are used to reduce spectral variance [17]. Recently we have also presented the complete theory for a Hermite function multitaper reassigned spectrogram, which has shown to significantly reduce the variance in the TF localisation estimates for transient signals [4]. Multitaper methods have also been explored earlier in connection to reassignment for longer FM signals [7], [12].

In this paper we present and evaluate multitaper Phase-Scaled Reassignment (mtPSR) techniques for relative phase estimation between two oscillating transient signals. This work extends on our Phase-Scaled Reassignment (PSR), shown to estimate phase-difference with high efficiency and accuracy for moderate SNR [18]. Section 2 details the multitaper reassigned cross-spectrogram with proposed novel RVs, and in section 3 we outline three novel approaches to reduce variance using the multitaper RVs. Evaluation of our methods are presented in section 4, and in section 5 we demonstrate the performance on measurements of electrical brain activity. Section 6 concludes the paper.

II. Multitaper Reassigned Cross-spectrogram

An oscillating transient signal is defined as

$$x(t) = g(t - t_0)e^{i2\pi f_0 t}, \quad t \in R \tag{1}$$

Thanks to the strategic research program ELLIIT and the Crafoord Foundation for financial support.

where t_0 is the time delay, f_0 the frequency, and $g(t)$ the real-valued Gaussian envelope function

$$g(t) = e^{-\frac{t^2}{2\sigma^2}}. \tag{2}$$

The signal $x(t)$ can be extended to a pair of signals

$$y_n(t) = A_n x(t) \mathrm{e}^{-i\phi_n}, \quad n = 1, 2 \tag{3}$$

where $y_1(t)$ and $y_2(t)$ have the same time delay and oscillating frequency but different amplitudes A_n and phases ϕ_n for $n = 1, 2$.

Next we define data windows $h_k(t)$, $k = 0 \dots K-1$ from the set of orthogonal Hermite functions [24],

$$h_k(t) = H_k(\frac{t}{\sigma}) e^{-\frac{t^2}{2\sigma^2}}, \quad k = 0 \dots K-1 \tag{4}$$

where σ is the width defining parameter of the taper. $H_k(t)$ is the physicist Hermite polynomial of order k defined as

$$H_k(t) = (-1)^k e^{t^2} \frac{d^k}{dt^k} e^{-t^2}, \quad k = 0 \dots K-1. \tag{5}$$

The short-time Fourier transform (STFT) of the signal $y_n(t)$ with use of the window $h_k(t)$ is

$$F_{y_n}^{h_k}(t, f) = \int y_n(s) h_k^*(s-t) e^{-i2\pi f s} ds \tag{6}$$

where * is the complex conjugate. All integrals run from $-\infty$ to ∞ if not specified. A reassigned cross-spectrogram of the signal pair $y_1(t)$ and $y_2(t)$ is defined as

$$RS(t, f) = \iint S_{12}(s, \xi) \delta(t - \hat{t}(s, \xi), f - \hat{f}(s, \xi)) ds \, d\xi \tag{7}$$

where $S_{12}(t, f)$ is the cross-spectrogram, and $\hat{t}(t, f)$ and $\hat{f}(t, f)$ define the RVs. The two-dimensional Dirac impulse function is defined as $\iint S(t, f) \delta(t - t_0, f - f_0) dt \, df = S(t_0, f_0)$. Different options for estimation of the cross-spectrogram and the RVs will be explored in Section IIA and III.

A. Novel multitaper reassignment vectors

Extending on our previous work on cross-spectrogram reassignment [17] and a multitaper reassigned spectrogram in [4], we now propose RVs for the multitaper cross-spectrogram

$$\hat{t}_k(t, f) = t + \Re \left(c_t \frac{F_{y_1}^{th_k} - \sigma^2 F_{y_1}^{\frac{dh_k}{dt}}}{F_{y_2}^{h_k}} \right), \tag{8}$$

$$\hat{f}_k(t, f) = f - \frac{1}{2\pi} \Im \left(c_f \frac{F_{y_1}^{\frac{dh_k}{dt}} - \frac{1}{\sigma^2} F_{y_1}^{th_k}}{F_{y_2}^{h_k}} \right) \tag{9}$$

where $\Re(.)$ and $\Im(.)$ denotes the real and imaginary operator, c_t and c_f are constants, and (t, f) is dropped in the STFTs for convenience. Based on the relation between the different STFTs, see [4], the following simplifications of the STFT expressions are found

$$F_{y_n}^{h_k} = A_n e^{-i\phi_n} F_x^{h_k} \tag{10}$$

$$F_{y_n}^{th_k} = A_n e^{-i\phi_n} (\sigma k F_x^{h_{k-1}} - \frac{\sigma^2 \beta}{2} F_x^{h_k}) \tag{11}$$

$$F_{y_n}^{\frac{dh_k}{dt}} = A_n e^{-i\phi_n} (\frac{k}{\sigma} F_x^{h_{k-1}} + \frac{\beta}{2} F_x^{h_k}) \tag{12}$$

where $F_x^{h_k}$ represents the STFT for the oscillating signal $x(t)$ in (1) and $\beta = t/\sigma^2 + i2\pi f$. With (10-12) the RVs will be simplified into

$$\hat{t}_k(t, f) = t - \Re(c_t \frac{A_1}{A_2} e^{-i\Delta\phi} (t + i2\pi\sigma^2 f)) \tag{13}$$

$$\hat{f}_k(t, f) = f - \Im(\frac{c_f}{2\pi} \frac{A_1}{A_2} e^{-i\Delta\phi} (\frac{t}{\sigma^2} + i2\pi f)) \tag{14}$$

where $\Delta\phi$ is the relative phase-difference between the signals, to be estimated. For all k, the choices of

$$c_t = c_f = \frac{A_2}{A_1} e^{i\Delta\phi} \tag{15}$$

result in perfectly localised energy in the cross-spectrogram at (t_0, f_0), i.e. the TF-spatial centre of the component, and thus giving a cross-spectrogram with low entropy.

III. Phase Estimation and mtPSR

This section proposes three ways to estimate the relative phase, $\Delta\phi$, for the mtPSR based on the novel RVs (8, 9). The key difference between the three variations, mtPSR1, mtPSR2, and mtPSR3, is at what stage in the estimation process the K different cross-spectrograms are brought together to form a single estimate $\hat{\Delta\phi}$. The different variations are detailed and summarized below as well as in Algorithm 1.

The mtPSR1 uses the multitaper cross-spectrogram,

$$S_{12}^m(t, f) = \frac{1}{K} \sum_{k=0}^{K-1} S_{12}^{h_k}(t, f), \tag{16}$$

where the absolute value of the cross-spectrogram for the single window $h_k(t)$ is defined as

$$S_{12}^{h_k}(t, f) = |F_{y_1}^{h_k}(t, f) (F_{y_2}^{h_k}(t, f))^*|. \tag{17}$$

The RVs are calculated as

$$\hat{t}_m(t, f) = \frac{1}{K} \sum_{k=0}^{K-1} \hat{t}_k(t, f), \tag{18}$$

$$\hat{f}_m(t, f) = \frac{1}{K} \sum_{k=0}^{K-1} \hat{f}_k(t, f) \tag{19}$$

before calculating the $RS(t, f)$ in (7). According to our previous work in [18], the $\hat{\Delta\phi}$ is obtained by evaluating the Rényi entropy (with $\alpha = 3$ and TF-domain area $\mathcal{A}$)

$$RE = \frac{1}{1-\alpha} \log_2 \iint_{\mathcal{A}} \left(\frac{RS(t, f)}{\iint_{\mathcal{A}} RS(s, \xi) \mathrm{d}s \, \mathrm{d}\xi} \right)^{\alpha} \mathrm{d}t \, \mathrm{d}f \tag{20}$$

Algorithm 1 Phase estimation according to the three proposed methods: mtPSR1, mtPSR2, mtPSR3

Input: $\{F_{y_n}^{h_k}(t,f)\}$, $\{F_{y_n}^{th_k}(t,f)\}$, $\{F_{y_n}^{\frac{dh_k}{dt}}(t,f)\}$, $\{\Delta\phi_c\}$ **Output:** $\hat{\Delta\phi}$

Calculate $S_{12}^{h_k}(t,f) = |F_{y_1}^{h_k}(t,f)F_{y_2}^{h_k}(t,f)^*|$ for $k = 0, ..., K-1$

[mtPSR1]
for all $\Delta\phi_c$ **do**
  for $k = 0$ to $K-1$ **do**
    Calculate $\hat{t}_k$, $\hat{f}_k$ (8, 9)
  end for
  Calculate S_{12}^m (16), and $\hat{t}_m$, $\hat{f}_m$, (19)
  Calculate RS (7), with S_{12}^m, $\hat{t}_m$, $\hat{f}_m$
  Evaluate $RE(\Delta\phi_c)$ (20)
end for
$\hat{\Delta\phi} = \arg\min_{\Delta\phi_c} RE(\Delta\phi_c)$

[mtPSR2]
for all $\Delta\phi_c$ **do**
  for $k = 0$ to $K-1$ **do**
    Calculate $\hat{t}_k$, $\hat{f}_k$ (8, 9)
    Calculate RS_k (7), with $S_{12}^{h_k}$, $\hat{t}_k$, $\hat{f}_k$
  end for
  $RS = \frac{1}{K}\sum_{k=0}^{K-1} RS_k$ (21)
  Evaluate $RE(\Delta\phi_c)$ (20)
end for
$\hat{\Delta\phi} = \arg\min_{\Delta\phi_c} RE(\Delta\phi_c)$

[mtPSR3]
for $k = 0$ to $K-1$ **do**
  for all $\Delta\phi_c$ **do**
    Calculate $\hat{t}_k$, $\hat{f}_k$ (8, 9)
    Calculate RS_k (7), with $S_{12}^{h_k}$, $\hat{t}_k$, $\hat{f}_k$
    Evaluate $RE(\Delta\phi_{c_k})$ (20)
  end for
  $\hat{\Delta\phi}_k = \arg\min_{\Delta\phi_{c_k}} RE(\Delta\phi_{c_k})$
end for
$\hat{\Delta\phi} = \angle(\sum_{k=0}^{K-1} e^{i\hat{\Delta\phi}_k})$ (22)

of reassigned cross-spectrograms, $RS(t,f)$, that are calculated using different candidate phase differences $\Delta\phi_c$ in (15) to compute the RVs. The candidate that minimises the Rényi entropy is chosen as $\hat{\Delta\phi}$.

In the mtPSR2, the RVs in (8,9) and the cross-spectrograms in (17) are brought together to form K different reassigned cross-spectrograms $RS_k(t,f)$ in (7). These are averaged to get a single multitaper reassigned cross-spectrogram

$$RS(t,f) = \frac{1}{K}\sum_{k=0}^{K-1} RS_k(t,f). \tag{21}$$

To get an estimate $\hat{\Delta\phi}$, the $RS(t,f)$ is evaluated using the Rényi entropy in the same way as for the mtPSR1.

Similarly, in the mtPSR3 K different $RS_k(t,f)$ are calculated from $S_{12}^{h_k}(t,f)$ and $\hat{t}_k(t,f), \hat{f}_k(t,f)$. But instead of bringing them together to a single multitaper reassigned cross-spectrogram, each $RS_k(t,f)$ is evaluated using the Rényi entropy. This gives K estimates $\hat{\Delta\phi}_k$ that are averaged to form a single estimate

$$\hat{\Delta\phi} = \angle(\sum_{k=0}^{K-1} e^{i\hat{\Delta\phi}_k}), \tag{22}$$

where $\angle(z)$ takes the angle of a complex number z.

IV. Evaluation

In this section the three mtPSR variations, mtPSR1, mtPSR2, and mtPSR3, are compared and evaluated. Real-valued oscillating transient signal pairs, $y_1(t)$ and $y_2(t)$, of lengths $N = 256$ with Gaussian envelopes are simulated, where the scaling of the window is $\sigma = 13$. All signals have equal amplitudes, $A_1 = A_2 = 1$, time delays $t_0 = 1$ s, and frequencies $f_0 = 20$ Hz, using sampling frequency $F_s = 128$ Hz. The phases, ϕ_1 and ϕ_2, are randomly generated from $\mathcal{U}(-\pi, \pi)$. White Gaussian noise is added to each signal, where the SNR is defined as

$$SNR = 10\log_{10}(\frac{A_1^2}{s^2}), \tag{23}$$

with s^2 as the noise variance. In Fig. 1 the signals are exemplified, with and without noise, for $\Delta\phi = \pi/3$. All

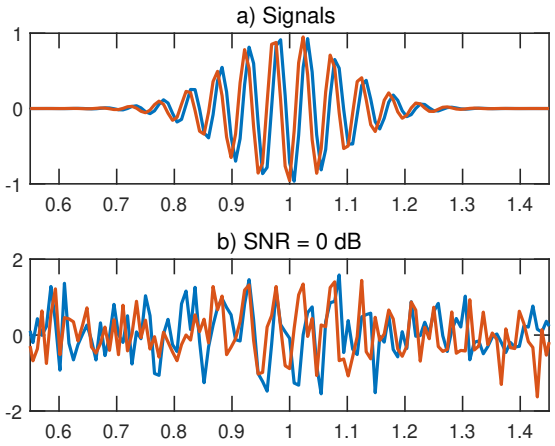

Fig. 1. Example of a simulated signal, $\Delta\phi = \pi/3$; a) without added noise; b) SNR = 0 dB.

simulations are run with FFT-length 1024, and the Hermite windows in the STFTs are assumed to be matched such that $\sigma_c = 13$. Thirty-two equidistant $\Delta\phi_c \in [-\pi, \pi[$ are evaluated such that each $\Delta\phi_c$ correspond to a time-shift of 1.53 ms for the considered signals. Moreover, the Rényi entropy is evaluated over the entire TF-plane.

In Fig. 2, we illustrate the different performances of the three variations when SNR $= 0$ dB. In Fig. 2a, the root mean squared error (RMSE) is depicted for different number of windows K. In Fig. 2b, the percentage of correct estimates, defined as $|\hat{\Delta\phi} - \Delta\phi| \leq 1.5\frac{2\pi}{32}$, is shown. This corresponds to an allowed error of 2.30 ms for the considered signals. For $2 \leq K \leq 4$, the mtPSR1 is the most accurate, but for $K \geq 7$ the accuracy of the method deteriorates. For $K \geq 5$ the mtPSR3 continuously improves and remains the most accurate. However, there is a trade-off between the gained accuracy and increase in computational load. Furthermore, since reassignment only is done once in mtPSR1, independent of K, it has the additional advantage of being less computationally complex per increase in K compared to mtPSR3. As such, in cases where computational efficiency is of importance the mtPSR1 is the superior option as it can achieve sufficient

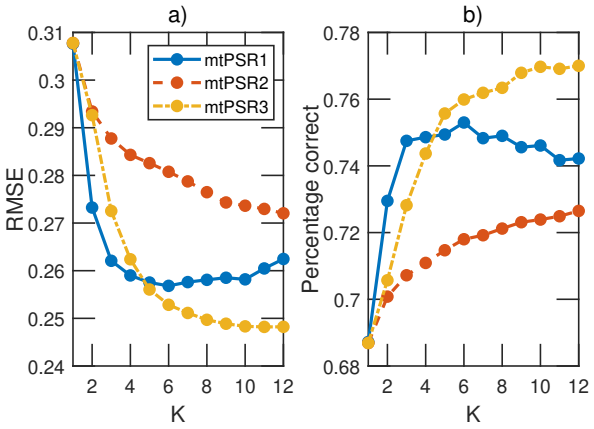

Fig. 2. Phase estimation results for different number of Hermite windows, 10 000 simulations and SNR = 0 dB; a) the root mean squared error (RMSE) of $\hat{\Delta\phi}$; b) the percentage of correct estimates.

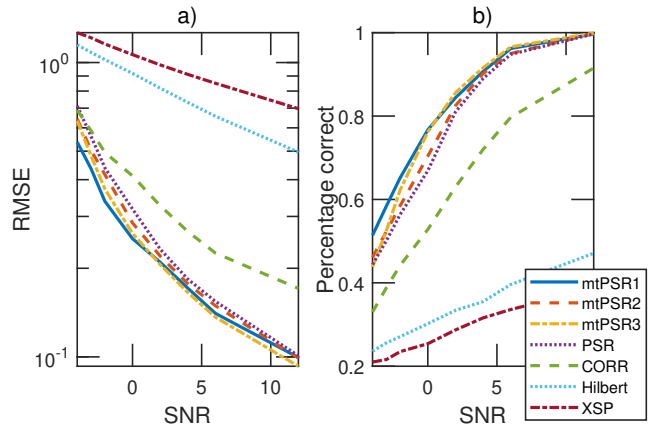

Fig. 3. Phase estimation results for different SNRs, for 1000 simulations and $K = 4$; a) the RMSE of $\hat{\Delta\phi}$; b) the percentage of correct estimates.

accuracy for a small K.

We therefore choose $K = 4$ as we continue to compare the methods to our previously proposed PSR method, as well as to several state-of-the-art methods: CORR, XSP [15] and the Hilbert transform, for different SNR. The cross-spectrogram of the XSP is computed using the matched Gaussian window, and for the maximum absolute value at each time point, the phase values are extracted and averaged. The Hilbert transform is used to find the instantaneous phase-differences $\hat{\Delta\phi}(t)$ [20], and the average is used as an estimate. CORR is evaluated for 32 different time-lags, and the estimate is chosen as the time-lag maximising CORR. In Fig. 3, all mtPSR variations are shown to be more accurate than the PSR method, which in turn is more accurate than the remaining state-of-art methods. As the PSR methods are TF-based measures, they have a clear advantage over time based measures such as CORR and Hilbert. Moreover, the mtPSR3 is slightly more accurate in high SNR. This is unsurprising as the mtPSR1 and mtPSR2 are restricted to find estimates $\hat{\Delta\phi}$ from a grid of candidates $\Delta\phi_c$, whereas the mtPSR3 can find estimates $\hat{\Delta\phi}$ between the

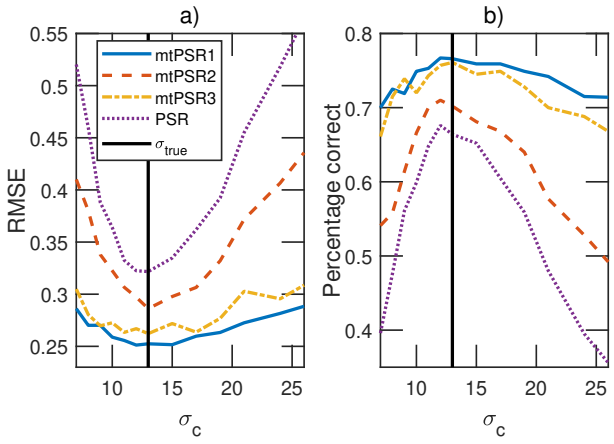

Fig. 4. Phase estimation results for different choices of scaling σ_c in the Hermite windows, for 1000 simulations, SNR = 0 dB and $K = 4$. The true σ is marked with a black line; a) the RMSE of $\hat{\Delta\phi}$; b) the percentage of correct estimates.

grid points.

The greatest advantage with the mtPSR in comparison to the PSR is its robustness to the matched-window assumption. In real-data settings, the scaling parameter, σ, of the Gaussian window might be unknown and difficult to estimate. In Fig. 4, SNR = 0 dB and the windows have been calculated with a scaling parameter σ_c that is different from the true scaling of the signal envelope σ_{true}. The accuracy is drastically reduced for the PSR if the matched window assumption is violated, whereas the accuracy of mtPSR1 and mtPSR3 is almost constant. For $K > 4$ this effect will be even more apparent.

V. Real Data Example

To illustrate performance for real data, 5 s of 20 Hz visual evoked potentials in EEG was studied. Data was recorded at electrodes in the 10-20 positions using a Neuroscan system with band-pass settings 0.3 and 50 Hz and sample rate 256 Hz. After recording, data was high-passed filtered at 5 Hz and down-sampled to $F_s = 64$ Hz.

The oscillations are expected to originate from electrodes at the visual cortex, i.e. electrodes O_1 and O_2, and propagate forward. Fig. 5 shows the estimated $\hat{\Delta\phi}$ between O_2 and all other channels for the PSR and mtPSR1 methods. The methods were applied with $\sigma = 11/12F_s$, and the signal amplitudes $\hat{A}_1$ and $\hat{A}_2$ were estimated as the maximum value of their respective spectrograms/multitaper spectrograms. The reassignment was done in a small window around the signal, and the Rényi entropy was evaluated in this same window. At channel O_2, both methods estimate approximately a zero phase difference compared to O_2, as expected. The largest phase-differences are found for channels at the frontal lobe for both methods, but the mtPSR method appears to give slightly more cohesive estimates.

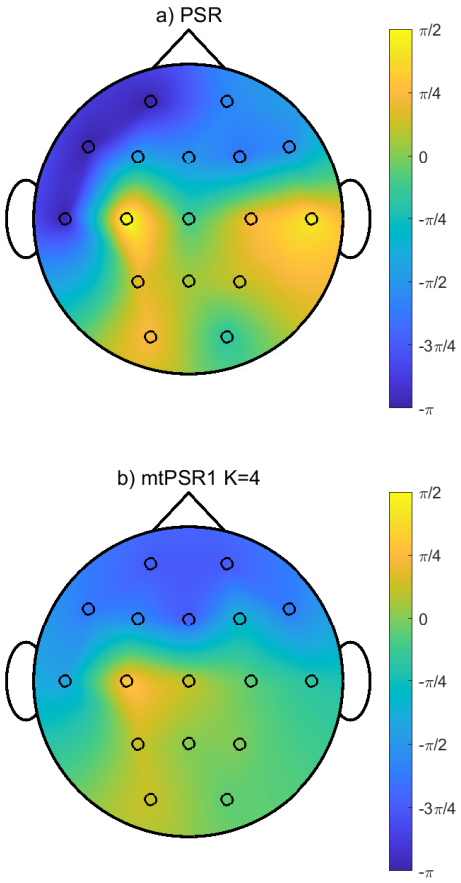

Fig. 5. The figures show the estimated $\hat{\Delta\phi}$ between O_2 and all other channels using; a) the PSR; b) mtPSR1 using $K = 4$ windows.

VI. Conclusion

The novel multitaper Phase-Scaled Reassignment method (mtPSR) is proposed and evaluated for robust estimation of phase difference between two short oscillatory transient signals. The performance of three different mtPSR variations are tested for the matched window case, i.e. known signal envelope, showing high accuracy for low SNR. Robust and precise phase delay estimates are obtained already for a few, around 4, windows, which makes the method computationally viable. Importantly, the mtPSR method also show robustness when the signal envelope is not known and estimated with some error. The mtPSR method give promising results when estimating the phase difference between different channels for visual evoked potentials component of noisy EEG data.

References

[1] M. Hansson-Sandsten and J. Brynolfsson, "The scaled reassigned spectrogram with perfect localization for estimation of Gaussian functions," *IEEE Signal Processing Letters*, vol. 22, no. 1, pp. 100–104, 2015.

[2] J. Brynolfsson and M. Sandsten, "Parameter estimation of oscillating Gaussian functions using the scaled reassigned spectrogram," *Signal Processing*, vol. 150, pp. 20–32, 2018.

[3] J. Brynolfsson, I. Reinhold, and M. Sandsten, "A time-frequency-shift invariant parameter estimator for oscillating transient functions using the matched window reassignment," *Signal Processing*, vol. 183, p. 107913, 2021.

[4] I. Reinhold and M. Sandsten, "The multitaper reassigned spectrogram for oscillating transients with Gaussian envelopes," *Signal Processing*, vol. 198, p. 108570, 2022.

[5] K. Kodera, C. de Villedary, and R. Gendrin, "A new method for the numerical analysis of nonstationary signals," *Physics of the Earth & Planetary Interiors*, vol. 12, pp. 142–150, 1976.

[6] F. Auger and P. Flandrin, "Improving the readability of time-frequency and time-scale representations by the reassignment method," *IEEE Trans. on Signal Processing*, vol. 43, pp. 1068–1089, May 1995.

[7] I. Daubechies, Y. G. Wang, and H.-T. Wu, "ConceFT: concentration of frequency and time via a multitapered synchrosqueezed transform." *Phil. Trans. R. Soc. A*, vol. 374, no. 20150193, 2016.

[8] K. Abratkiewicz and P. Samczyński, "Multitaper time-frequency reassigned spectrogram in micro-Doppler radar signal analysis," in *2021 Signal Processing Symposium (SPSympo)*, 2021, pp. 1–5.

[9] N. Laurent, M. A. Colominas, and S. Meignen, "On local chirp rate estimation in noisy multicomponent signals: With an application to mode reconstruction," *IEEE Trans. on Signal Processing*, vol. 70, pp. 3429–3440, 2022.

[10] K. Czarnecki, D. Fourer, F. Auger, and M. Rojewski, "A fast time-frequency multi-window analysis using a tuning directional kernel." *Signal Processing*, vol. 147, pp. 110 – 119, 2018.

[11] D. Fourer, F. Auger, and G. Peeters, "Local AM/FM parameters estimation: Application to sinusoidal modeling and blind audio source separation," *IEEE Signal Processing Letters*, vol. 25, no. 10, pp. 1600–1604, 2018.

[12] J. Xiao and P. Flandrin, "Multitaper time-frequency reassignment for nonstationary spectrum estimation and chirp enhancement," *IEEE Trans. on Signal Processing*, vol. 55, no. 6, pp. 2851–2860, 2007.

[13] W. Bao, F. Li, and Z. Chen, "Generalized transient-squeezing transform: Algorithm and applications," *IEEE Trans. on Instrumentation and Measurement*, vol. 71, pp. 1–10, 2022.

[14] Z. He, X. Tu, W. Bao, Y. Hu, and F. Li, "Second-order transient-extracting transform with application to time-frequency filtering," *IEEE Trans. on Instrumentation and Measurement*, vol. 69, no. 8, pp. 5428–5437, 2020.

[15] L. Cohen, *Time-Frequency Analysis*, ser. Signal Processing Series. Upper Saddle River, NJ, USA: Prentice-Hall, 1995.

[16] M. Sandsten, R. Anderson, I. Reinhold, and J. Brynolfsson, "The matched reassigned cross-spectrogram for phase estimation," in *Proceedings of the ICASSP*. Barcelona, Spain: IEEE, 2020, virtual.

[17] M. Sandsten, R. Anderson, I. Reinhold, B. Bernhardsson, C. Bergeling, and M. Johansson, "A novel multitaper reassignment method for estimation of phase synchrony," in *Proceedings of the EUSIPCO*, Dublin, Ireland, 2021, virtual.

[18] M. Åkesson and M. Sandsten, "Phase reassignment with efficient estimation of phase difference," in *Proceedings of the EUSIPCO*, Belgrade, Serbia, 2022.

[19] O. Keding and M. Sandsten, "Robust phase difference estimation of transients in high noise levels," in *Proceedings of the EUSIPCO*, Belgrade, Serbia, 2022.

[20] C. J. Stam, G. Nolte, and A. Daffertshofer, "Phase lag index: Assessment of functional connectivity from multi channel EEG and MEG with diminished bias from common sources." *Human Brain Mapping*, vol. 28, no. 11, pp. 1178–1193, 2007.

[21] Y. Zhao and Y. Su, "Synchrosqueezing phase analysis on micro-doppler parameters for small UAVs identification with multichannel radar," *IEEE Geoscience and Remote Sensing Letters*, vol. 17, no. 3, pp. 411–415, 2020.

[22] R. Wang, M. Xiang, B. Wang, and C. Li, "Nonlinear phase estimation and compensation for FMCW ladar based on synchrosqueezing wavelet transform," *IEEE Geoscience and Remote Sensing Letters*, vol. 18, no. 7, pp. 1174–1178, 2021.

[23] D. J. Thomson, "Spectrum estimation and harmonic analysis," *Proceedings of the IEEE*, vol. 70, no. 9, pp. 1055–1096, Sept 1982.

[24] I. Daubechies, "Time-frequency localization operators: A geometric phase space approach," *IEEE Trans. on Information Theory*, vol. 34, no. 4, pp. 605–612, 1988.